NASA CONTRACTOR REPORT 166396

(NASA-CR-166396) AEROSOUND FROM CORNER FLOW AND FLAP FLOW (California Univ.) 41 p
HC A03/MF A01
CSCL 20A

N82-32081

Unclas
G3/71 28840

Aerosound From Corner Flow and Flap Flow

W. C. Meecham

CONTRACT NAS2–10590
July 1982

NASA

NASA CONTRACTOR REPORT 166396

Aerosound From Corner Flow and Flap Flow

W. C. Meecham
Mechanics Development Company
Pacific Palisades, California
and
School of Engineering and Applied Science
University of California, Los Angeles
Los Angeles, California

Prepared for
Ames Research Center
under Contract NAS2-10590

National Aeronautics and
Space Administration

Ames Research Center
Moffett Field California 94035

ORIGINAL PAGE IS
OF POOR QUALITY

PART I

AEROSOUND FROM CORNER FLOW AND FLAP FLOW.*

BY

W.C. Meecham,† School of Engineering and Applied Science
University of California, Los Angeles, California 90024

ABSTRACT

The model consists of a vortex moving around a corner in an imcompressible, potential flow. A possible explanation of the typically small Strouhal numbers seen here is the vortex image retarding-effect. The model surface pressures, sound pressures (using Curle's theory) and Mach number dependencies agree well with wind tunnel experiments. A double pressure peak is found in the model (credited to image action) which is qualitatively similar to measured sound correlations. We discuss incompressible-flow aerosound calculations.

*Presented as Paper 81-2039 at the AIAA 7th Aeroacoustics Conference, Palo-Alto, CA, Oct 5-7, 1981
* This work was supported by the Lowspeed Aircraft Research Branch of the NASA-AMES Research Center
Copywright (c) 1981 by W.C. Meecham
†Professor, Department of Mechanics and Structures; Associate Fellow, AIAA.

Introduction

Residents around airports are often exposed to high noise levels by commerical jet planes during landing operations. The problem is aggravated by the small glide angles necessary during approach. (Though the noise produced at take-off is much greater, it doesn't last as long at ground level because of higher climb-out angles.)

It is also true that at landing, engines are operated at reduced thrust, and consequently high lift, airframe components, such as slots and flaps, may become noise sources of importance. Recent work by Ahtye, Miller and Meecham [1], Fink and Schlinker [2] and Kendell and Ahtye [3] has indicated that of the various possible airframe noise sources, the side edges of flaps seem to dominate. This is presumably because of the span-wise flow caused by the pressure differential between the high pressure, lower flap surface and the lower pressure, upper flap surface. The importance of this noise source is emphasized by the fact that the eddy structure in this side edge region shows a correlation length of order the flap chord, which is considerably greater than the typical turbulent eddy correlation lengths found elsewhere in the flow. Such larger correlation lengths enhance the radiated sound as will be seen below, see Miller, Meecham and Ahtye [4] and Miller [5].

Earlier work (Hayden [6]) had emphasized as an important noise source region the trailing edges of flaps and wings. However, our measurements, [1], indicate that the noise from the trailing edges of flaps is small (in our case undetectable) except at the very corners of the flap, inboard and outboard. Earlier, more extensive measurements by Yu and Tam [7] also indicated that such trailing edge noises were quite small. This result may be regretted, for it is clear that the geometry of a trailing edge is considerably simpler than that of separated flow around corners. In the latter case we must contend with swirling flows, corners and other complications.

We present here a model problem calculation which, hopefully, will be applicable to other problems involving the generation of aerosound by turbulent flow around corners. Our application is of course the flap edge, and we use the language of that problem.

To begin the treatment, and we must first deal with the flow around a blunt object. One could construct an elaborate, empirical treatment for the discussion of aerosound from such flows; obviously a more analytical approach would be desirable. One simplified model for these flow processes involves the use of moving vortices imbedded in potential flows (for an inviscid, incompressible fluid). The main advantage here is that one has available conformal mapping procedures. The treatment leads naturally to a two dimensional statement of the problem. This type of development forms but a model of the actual, very complicated flow problem.

The physical flow consists of distributed vorticity with all of the complexities inherent in the inhomogeneous turbulent process. If we are to make progress using an analytical treatment a simplier model such as described above is clearly needed. Among papers adopting such methods we may cite: For the fluid mechanics, Clements [8]; for flow about a half-plane with application to aerosound, Howe [9], [10] and Hardin [11]. In Refs. [9] and [11] a special and simple procedure due to Howe is employed in the calculation. This procedure, if complete, permits a considerable simplification in the determination of the aerosound. However, if we use it, when the two dimensional problem is adapted to three dimensional geometries it appears that the sound power goes as the fourth power of the flow Mach number; as is known, Lighthill [12] finds for volume sound an eight power of the Mach number and Curle [13] produces the well-known sixth power dependence for surface sound. These apparent difficulties persuaded the author to carry out calculations here using standard Lighthill-Curle theory. As will be seen below the surface sound yields a sixth power dependence, with a dipole augular distribution.

A further difficulty with some earlier work is the following: In an exact theoretical statement of the problem, the fields for an incompressible flow should be recovered. Thus, if exactly

incompressible quantities are used, one should find no radiated sound when including both volume and surface sound. That doesn't appear to be the case in the cited references. It is expected for the Lighthill-Curle theory that such a result should follow.

We propose to use incompressible flow quantities for the calculation of aerosound radiated by the flap surface.

In the standard treatment of the problem one finds sound radiated as a result of two source mechanisms: Volume sound and surface sound. If we use the statement of the radiated sound in terms of density changes, then for incompressible flow these two integral contributions should be equal and opposite, since of course there is no density change in an incompressible fluid. In the course of the Lighthill-Curle discussion, what is really an arbitrary parameter, a_0, is introduced. It is convenient ordinarily to choose for that parameter the ambient speed of sound. For an incompressible flow problem we are free to make an arbitrary choice. If one does so, then the surface and volume sound must just cancel one another. We will here calculate the surface sound radiated by our model of the process. We do so using incompressible flow quantities. The rationale which we employ, and which is implicit in other similar treatments of the problem, is that the field quantities near the surfaces producing dipole sound, are approximately the same for an incompressible fluid and for a slightly compressible one under similar conditions. Thus we may use the simpler incompressible quantitites in the calculation. These questions are discussed more fully in Appendix A.

Figure 1 shows a sketch of the wing and deployed flap, viewed from the underside of the wing. Two average, streamlines are shown. Viewed from the aircraft, the flow proceeds along the wing and then spills (or is pushed by the high pressure on the underside of the flap) around the outboard blunt edge of the flap. Figure 2 is a close-up of the flow around this blunt edge and also shows the coordinate system used: The x_1 axis lies along the trailing edge of the flap; the x_3 axis lies along the outboard, lower edge of the flap and x_2 is perpendicular to the underside of the flap. A field point $\underset{\sim}{x}$ is shown. The dotted line from

$\underline{x}$ is its projection on the $x_1 - x_2$ plane, ϕ is the (azimuthal) angle of that projection from the x_2 axis and θ is the polar angle, measured from the x_3 axis. Figure (3a) shows the model, potential flow about the flap corner, with an imbedded vortex. Figure (3b) shows the uniform flow with the vortex (and its image) in the transformed plane (see below).

In the spanwise flow about the blunt end of the flap, it was found in Refs. [1], [4] and [5], that most of the sound was radiated from the underside of the flap, that is the surface on which the flow first impinges, the horizonial surface in Fig.(3a). This was determined through the use of cross-correlation techniques. The upper side of the flap showed little detectible, radiated sound. Our model here will consist of a vortex moving around from the lower horizonal surface to the vertical surface. We make no effort to construct the flow around the upper horizonal surface, the dashed line in Fig (3a), for reasons just cited. Typically one thinks of flow separation at the corners, producing vortices. In our case, from the cross correlation measurements taken at the lower surface, it's clear that the vortex when formed is large enough and diffuse enough so that it has a major effect on the lower surface, thus not appearing <u>just</u> at the corner. The qualitative characteristics of the flow to be used here are similar to those measured around edges by Francis and Kennedy [14]. In our experiments we didn't actually place pressure sensors at the blunt edge of the flap, in Fig.(3a) the lower portion of the vertical surface. But we expect that when such experiments are performed, applicable sound will be found originating from this region as well. We include it in our treatment.

II. Theory of Airframe Surface Noise

It is not necessary to review completely the standard aerosonic theory. We content ourselves with a few points of importance in the discussion and with results. Lighthill [12] begins with the exact equations of motion for a fluid. In his treatment he models the propagation of sound in a fluid at rest. He has, at an intermediate stage,

ORIGINAL PAGE IS
OF POOR QUALITY

$$\frac{\partial^2 \rho}{\partial t^2} - a_0^2 \nabla^2 \rho = \frac{\partial^2}{\partial x_i \partial x_j} T_{ij}$$

$$T_{ij} = \rho u_i u_j + p_{ij} - a_0^2 \rho \delta_{ij} \qquad (1)$$

where ρ = density, p_{ij} = compressive stress tensor, a_0 = speed of sound in the ambient fluid (though a_0 may be chosen arbitrarily), v_i = the components of the fluid velocity in the direction x_i ($i = 1,2,3,$); we sum over repeated indices. Equation (1) is solved for free-turbulence flows by Lighthill and for turbulence in the presence of rigid boundaries by Curle [13]. Curle obtained, for the surface contribution to the density change (in the situation where $x>>\lambda>>L$ with λ the wave length of the most strongly radiated sound and L a typical dimension of the solid body of interest), the following

$$x_i \left(4\pi a_0^3 x^2\right)^{-1} \frac{\partial}{\partial t} \int_S P_i \left(\underline{y},\ t - \frac{r}{a_0}\right) dS(\underline{y}) \qquad (2)$$

where $\underline{y}$ is the source position vector, $r = |\underline{x} - \underline{y}|$ and $\underline{x}$ is the field point. The source system is said to be compact if $\lambda>>L$. Below it is understood that the radiated signal is delayed by r/a_0; we shall not always show the delay explicity.

The P_i are the components of the force exerted by the surface on the surrounding fluid. The integral is to be carried out over the entire surface. For simplicity in our application we assume that the chord, C, is small compared with the sound wavelength and that we are far away compared with C. The dimension of the flap in the span-wise direction may be larger than the sound wavelength. However, our noise producing eddies have a scale in the span-wise direction of order the thickness of the flap, see Refs. [1] and [4]; it is known that the dipole sound vanishes for turbulence over a flat plate. Thus, far from the flap edge, we expect little surface-sound contribution. Consequently, we have assumed that the sources are compact for the

ORIGINAL PAGE IS
OF POOR QUALITY

entire radiating portion of the surface.

Our model consists of a vortex (plus its image) imbedded in a potential flow around a corner. We introduce a complex variable

$$z = y_1 + iy_2 = Re^{i\theta}, \quad (-\pi \leq \theta \leq \frac{\pi}{2}).$$

Physical space may be transformed, as shown in Fig. 3b, with $\lambda = \xi + i\eta$, using

$$\lambda = \left(ze^{i\pi}\right)^{2/3} \tag{3}$$

Assuming a uniform flow in the transformed plane, the complex potential is

$$W(\lambda) = -A\lambda - \frac{i\Gamma}{2\pi} \ln (\lambda - \lambda_0) + \frac{i\Gamma}{2\pi} \ln (\lambda - \lambda_0^*), \tag{4a}$$

here $\lambda_0 = \xi_0 + i\eta_0$ the transformed vortex position, A determines the magnitude of the uniform flow in the negative ξ direction and the complex conjugate is indicated throughout by an asterisk. The Γ is the circulation strength of the vortex. Also $z_0 = y_{01} + iy_{02} = R_0 e^{i\theta_0}$ is the vortex position in the physical plane and is related to λ_0 by Eq. (3). We write the equations in dimensionless form using for velocity βU_0 where in our physical problem U_0 is the speed of the free stream and βU_0 is the speed of the flow in the span-wise direction (rolling over the edge of the flap). Here β is typically of order unity and is to be determined later. For the dimension of length we use D the thickness of the flap, and for the mass, $\rho_0 D^3$. Our measurements, see Refs. [1] and [4], show correlations with lengths of order D in the span direction. We suppose from the known characteristics of the vortices generated by separation, and from the physics of the problem that

$$A = \beta U_0 D^{1/3}$$

and

$$(\Gamma/2\pi) = \beta U_0 D \tag{4b}$$

setting the constants of proportionality equal to one. It will be noted that we retain but one adjustable parameter, β, thus limiting the (sometimes suspect) freedom to adjust the theory to the experiments. The

ORIGINAL PAGE IS
OF POOR QUALITY

equations may be conveniently made dimensionless by setting $A = \Gamma/2\pi = \rho_0 = 1$. The Eq. (4a) then becomes

$$W(\lambda) = -\lambda + i \ln [(\lambda - \lambda_0^*)/(\lambda - \lambda_0)]. \qquad (5)$$

To avoid the dread notational proliferation we use the same notation for dimensional and for dimensionless quantities; the latter may be identified by the apparent failure of dimension checks.

We find the components of the velocity in the physical plane in the usual way

$$\dot{y}_1 - i\dot{y}_2 = \frac{dW}{d\lambda}\,\frac{d\lambda}{dz} = \left[-1 + i(\lambda - \lambda_0^*)^{-1} - i(\lambda - \lambda_0)^{-1}\right] \frac{2}{3}\, e^{i2\pi/3}\, z^{-1/3} \qquad (6)$$

In the absence of the vortex the flow is steady and from Eq.(6) (without the vortex terms) we see the speed falls off as $R^{-1/3}$. The flow becomes time dependent, with a vortex present because the vortex moves. Its motion is essentially the velocity of its center as determined by the potential flow and the image vortex plus a correction term, according to Routh's rule [see Ref.(8)]; we find

$$\dot{y}_{01} - i\dot{y}_{02} = \left\{\left[-1 + i\,(\lambda - \lambda_0^*)^{-1}\right] \frac{d\lambda}{dz} - \frac{i}{2}\,\frac{d^2\lambda}{dz^2}\Big/\frac{d\lambda}{dz}\right\}_{z = z_0} \qquad (7)$$

taking real and imaginary parts,

$$\begin{matrix}\dot{y}_{01} \\ \dot{y}_{02}\end{matrix} = \frac{2}{3}\left[-R_0^{-1/3} + \left(R_0 \sin \frac{2}{3}\,(\theta_0 + \pi)\right)^{-1}\right] \begin{Bmatrix}\cos \frac{1}{3}\,(2\pi - \theta_0) \\ -\sin \frac{1}{3}\,(2\pi - \theta_0)\end{Bmatrix} \qquad (8)$$

$$+ (6R_0)^{-1} \begin{Bmatrix}\sin \theta_0 \\ -\cos \theta_0\end{Bmatrix}$$

ORIGINAL PAGE IS
OF POOR QUALITY

where upper and lower quantities go together. We solve these Eqs.(8) numerically, Fig. 4; note that the solution depends upon the initial position of the vortex; in our case we take t = 0 when the vortex crosses the symmetry line, $\theta_0 = -45^0$. The orbit (a) has $R_0 = 4$ initially; the orbit (b) has $R_0 = 2$ initially and shows the vortex moving more slowly than (a) because of the retarding effect of the vortex image; the orbit (c) approaches the wall closely enough so that the vortex is returned upstream and doesn't circumnavigate the corner; the orbit (d) shows the vortex close enough to the wall so that it moves counter to the motion of the potential flow. Orbits farther out show rapidly reducing sound fields: closer orbits return upstream and don't produce important characteristics of the flow. We may introduce additional vortices on the chosen orbit to model the flow process. We introduce them at a rate equal to the peak frequency observed in the sound field. We measured (see Refs. [1], [4] and [5]) the cross correlation of the surface pressure with the radiated sound pressure. In Appendix B we show that oscillations in the correlation function can be used to determine this peak frequency.

III. Aerosound Generated By Corner Flow

First note that Eq.(2) in dimensionless form becomes

$$\rho - 1 = \frac{Cx_i}{4\pi a_o^3 x^2}\left[\delta_{i2}\frac{\partial}{\partial t}\int_{-\infty}^{0}(p_1 + p_2)dy_1\Big|_{y_2=0} - \delta_{i1}\frac{\partial}{\partial t}\int_{0}^{\infty}(p_1 + p_2)dy_2\Big|_{y_1=0}\right]. \tag{9}$$

The pressure for inviscid flows is given by

$$p = K - \frac{1}{2}|\underline{u}|^2 - \partial\phi/\partial t,$$

$$p_1 = -\frac{\partial\phi}{\partial t}, \quad p_2 = -\frac{1}{2}|\underline{u}|^2, \quad \underline{u} = \dot{y}_1\hat{i} + \dot{y}_2\hat{j} \tag{10}$$

ORIGINAL PAGE IS
OF POOR QUALITY

The force exerted on the fluid by the boundary [components P_i in Eq.(2)] is given by the pressure force normal to the surface.

Note that the positive direction for the field point $\underline{x}$ is downward and to the left, left being upstream in the flow, as indicated in Fig.3a. In such two dimensional problems the pressures and velocities are independent of the coordinate direction along the edge of the flap, that is normal to the page in Fig. 3a. Consequently the surface integral along that direction is simply the (nondimensional) chord length C as indicated by the coefficient in Eq.(9). In Eq.(10) $\hat{i}$ and $\hat{j}$ are unit vectors along the axes. For this flow the velocity potential is obtained from

$$\phi = \text{Re } W, \tag{11}$$

where Re stands for real part, and below Im for imaginary part. Using Eqs. (5) and (11) we have

$$\frac{\partial \phi}{\partial t} = - 2 \text{ Im } \left[(\lambda - \lambda_0)^{-1} \frac{\partial \lambda_0}{\partial t} \right] \tag{12}$$

Note that the time dependence is contained entirely in the position of the vortex in the physical plane, z_0, or equivalently in its position in the transformed plane, λ_0. For the integrals we need, see Eq.(9), the derivative of the pressure from Eqs.(10) and (12) is

$$\frac{\partial p_1}{\partial t} = 2 \text{ Im } \left[(\lambda - \lambda_0)^{-2} \left(\frac{\partial \lambda_0}{\partial t} \right)^2 + (\lambda - \lambda_0)^{-1} \frac{\partial^2 \lambda_0}{\partial t^2} \right] \tag{13}$$

Think of substituting Eq.(13) for the derivative of p_1 in Eq.(9) (note that the derivatives of λ_0 are parameters in the integration). Both integrals of the second term in Eq.(13) will be divergent, referring to Eq.(5). Of course we might cut off the integrals by recognizing that the compactness of the source is violated for z sufficiently large. But if so these terms would dominate the result, being dependent as would be the case on a length of order the wave length of the sound, or the distance to the field point, both much larger than other lengths in the

ORIGINAL PAGE IS
OF POOR QUALITY

calcuation. This would not yield a sensible physical result for the radiated sound.

But the volume has a correspondingly divergent contribution (see the discussion in Appendix A) just cancelling this surface contribution. Accordingly we drop the second term in Eq.(13).

We designate the contribution of P_1 to the density change by $(\rho - 1)_1$. The integrals involved are of elementary form.

We find for this part of the density change

$$(\rho - 1)_1 \simeq \frac{3C\chi_i}{8a_c^3 x^2}\left\{\delta_{i2}\ \mathrm{Re}\left[\left(\frac{\partial\lambda_0}{\partial t}\right)^2 \lambda_0^{-1/2}\right] - \delta_{i1}\ \mathrm{Im}\left[\left(\frac{\partial\lambda_0}{\partial t}\right)^2 \lambda_0^{-1/2}\right]\right\} \tag{14}$$

Turn now to the pressure contribution from velocity changes, designated P_2, see Eq.(10)

For this contribution of the surface pressure, P_0, to the dipole, surface sound we need the square of the fluid velocity. Of course by construction the normal component of fluid velocity will vanish on the horizonal and vertical surfaces.

We take the square of the absolute value of Eq.(6); since after intergrating the pressure we must take the time derivative, we may neglect the term independent of λ_0. It is seen that all of the intergrals may be evaluated using standard contour integration methods. We find for the pressure integrals over the surface the result

$$\frac{\partial}{\partial t}\int_{-\infty}^{0} P_2\ (y_1,\ y_2 = 0)\ dy_1 + i\,\frac{\partial}{\partial t}\int_{0}^{\infty} P_2\ (y_1 = 0,\ y_2)\ dy_2 = \frac{\partial}{\partial t}\left[\lambda_0^{-1/2}\ (4i - 2i\ \lambda_{0i}^{-1} + \lambda_0^{-1})\right] \tag{15}$$

where $\lambda_0 = \lambda_{0r} + i\lambda_{0i}$

ORIGINAL PAGE IS
OF POOR QUALITY

Substituting and drawing these results together we have for the density change in the sound field the results, in dimensionless form,

$$\rho - 1 = [C \sin \theta/(a_0^3 x)] \cdot [G_H \cos \Phi + G_V \sin \Phi] \tag{16}$$

with

$$- G_H = F_{1H} + F_{2H}, \quad - G_V = F_{1V} + F_{2V}$$

$$\begin{pmatrix} F_{1H} \\ F_{1V} \end{pmatrix} = \frac{u_0^2}{6R_0} \begin{pmatrix} \cos [2\phi_0 + \theta_0] \\ -\sin [2\phi_0 + \theta_0] \end{pmatrix} \tag{17}$$

$$\begin{pmatrix} F_{2H} \\ F_{2V} \end{pmatrix} = u_0 (9 R_0^{4/3})^{-1}$$

$$\cdot \left\{ \left(-2 + \lambda_{0i}^{-1} \right) \begin{pmatrix} -\cos [\frac{1}{3} (\pi + \theta_0) - \phi_0] \\ \sin [\frac{1}{3} (\pi + \theta_0) - \phi_0] \end{pmatrix} \right. \tag{18)(19}$$

$$+ \frac{3}{2} R_0^{-2/3} \begin{pmatrix} -\sin (\phi_0 - \theta_0) \\ \cos (\phi_0 - \theta_0) \end{pmatrix}$$

$$\left. + \frac{2}{\lambda_{0i}} [\cos \phi_0 + \sin \phi_0 \cot \tfrac{2}{3} (\pi + \theta_0)] \begin{pmatrix} -\cos \frac{1}{3} (\pi + \theta_0) \\ \sin \frac{1}{3} (\pi + \theta_0) \end{pmatrix} \right\}$$

$$\phi_0 = \tan^{-1} (\dot{y}_{02}/\dot{y}_{01}) - \theta_0 \tag{20}$$

$$u_0 = (\dot{y}_{01}^2 + \dot{y}_{02}^2)^{1/2} \tag{21}$$

Here ϕ_0 is the angle between the vortex velocity vector, which lies in the first quadrant, and the vortex radius vector. In Eqs. (17)-(19) upper and lower values go together, respectively. The angle θ here is the polar angle measured from the (outboard) corner of the flap edge; Φ is the azimuthal angle. The senses of the angles are indicated in the sketch, Fig.2. We also show there the axes and their senses for the field vector $\underline{x}$. The application of most interest here is that of a flap deployed from a wing surface. We have then approximately $\Phi = 0$, and $\theta = (0, \pi)$, being zero when the field point is up stream. For this application the dipole sound generated by the edge, of width D, of the flap surface (what we have termed the vertical-surface contribution) will vanish, as we see from Eq.(16) with $\Phi = 0$. We concentrate our attention on this simplified case.

The surface pressure, P_0, is readily found using Eq.(10) substituting using Eqs.(6) and (11) for the velocity potential. The result is, up to an arbitrary hydrostatic pressure, on the surface [where by Eq.(3) we see that λ is real]

$$P_0 = -2\,(9R^{2/3})^{-1}\,[-1 + 2\lambda_{0i}\,|\,\lambda - \lambda_0\,|^{-2}]^2 \qquad (22)$$

$$+ \frac{4u_0}{3R_0|\lambda-\lambda_0|^2}\,[\lambda\lambda_{0i}\cos\phi_0 + \lambda\lambda_{0r}\sin\phi_0 - |\lambda_0|^2\sin\phi_0]$$

The pressure due to the potential flow alone may be obtained by letting R_0 be indefinitely large. In our pressure plots in the next section we we use this latter pressure as the reference.

As suggested earlier, in our model we may use a series of vortices, essentially set up by the separation process but, in the nature of the geometry, reaching back upstream from the separation point. These vortices are, from measurements in Refs. [1] and [4], found to be essentially, statistically independent of one another; thus we can add intensity effects. The instantaneous sound intensity at a distance x

from the corner is easily found to be, now using βU_0, D and ρ_0 to define the dimensions (for one vortex)

$$I = \frac{(\beta U_0)^6 \rho_0 c^2}{x^2 a_0^3} \left(\sin^2 \theta\right)[G_H \cos \Phi + G_v \sin \Phi]^2 \qquad (23)$$

The mean intensity is found by averaging this function over the period of the vortex shedding and including the overlap of the tails of the other vortex functions which may occur. In our applications, and in general for directly-overhead, flyover flap noise, we take as indicated $\Phi = 0$, $\theta = (0, \pi)$, see Fig. 2. In the result, Eq.(23), the quantities G_H and G_v are universal functions of dimensionless arguments varying only with the initial position of the orbit of the vortex. Even this position, as discussed, may not be widely varied.

IV. Computation Compared with Experiments, and Conclusions

The computations required for the theory described here are not extensive. What we report was done conveniently on a hand calculator.

The vortex orbits shown in Fig.4, calculated using Eq.(8), emphasize regions nearer to the corner. Generally speaking when $R_0 >> 1$, we no longer expect the model to represent the important characteristics of the physical flow, so the orbits then are not of interest; we do not show those portions. A further comment or two on the orbits will be be helpful. We shall choose the orbit (b) as the one with the qualitative characteristics for the radiated sound most closely approaching the observed ones. There is a metastable point for the vortex at $R_0 \simeq 1.4$ and $\theta_0 = -45^0$; the vortex (b) approaches this point, oscillates slightly near it (not seen on the scale of Fig.4) and then is sent back upstream. As explained, in these pressure plots we choose t = 0 when the vortex passes the line $= -45^0$.

Consider the near field pressure p_0 calculated using the orbit information already discussed and Eq.(22). We show p_0 in Fig.5 (using

the right hand vertical scale). The pressure is measured on the surface at the point $y_1 = -0.5$, $y_2 = 0$. This position corresponds roughly to our flap measurement positions in the experiments reported in Refs. [1], [4] and [5]. We show the surface pressure in Fig.5 for the orbits (a) and (b). The larger orbit shown in the figure, indicated by $R_0 = 4$, shows a single peak in time, along the horizontal axis (all quantities in dimensionless form).

As the vortex approaches the surface point the potential flow is modified by the vortex flow. The velocities at the surface are reduced and thus the pressure is increased. (It should be noted that we have taken for the pressure reference the potential flow value with no vortex, at the point in question. It amounts, in dimensionless form, to adding 0.35 to the calculated values.) The more interesting surface pressure for the closer orbit (b) is also shown in the figure. It is noted that there are two peaks; they appear for the following reason: As the vortex approaches the surface the combination of it with its image reduces the flow speed (by cancelling some of the potential flow) thus increasing the pressure. As the vortex moves past the bisecting line the images are poorly defined and the result is a reduction in the pressure because of increased fluid velocities at the measuring point. Then as the vortex passes the corner the image again becomes better defined and a corresponding increase in pressure is seen again. It should be noted here that the speed of the vortex is considerably slowed by the action of its images. Consequently the time of occurrance of these effects is relatively large, as can be seen in the dimensionless forms and as shown in Fig.5; thus in dimensionless form the time delay between the two peaks mentioned here is approximately 25 units.

This last characteristic leads to an interesting conclusion from this work for general fluid flows. The time characteristic just described is the inverse of the Strouhal, St, number. As is known St numbers are typically less than one for many flows, sometimes considerably less. The vortex street behind a cylinder has a St number of 0.2, a dimensionless period of 5. The reason for such low St numbers may in general be the phenomenon observed here: The vortex image slows the vortex motion, thus increasing the period of the fluctuating process.

Turn now to the aerodynamic sound generated by these fluctuating pressures. We show in Fig. 5 the dimensionless and normalized density change, see Eq.(16),

$$(\rho - 1)\, a_0^3\, x/(C \sin\theta) = G_H = -(F_{1H} + F_{2H}) \tag{24}$$

This is proportional to the density change for $\phi = 0$. This we observe the sound in the plane of the flat edge. This is approximately the plane in which most of our measurements have been made. (Also note the change of sign, in Eq.(24), in the sound field density.) Radiated sound for the farthest orbit (a) shows one negative and one positive peak, widely spaced and very broad. This orbit does not approximate well the vortex activity around the flap edge. We shall emphasize the closer orbit (b), calculations for which are also shown in Fig.5.

For this preliminary application of the theory to the available data we restrict to but one vortex. Referring to Fig.5 in the orbit $R_0 = 2$ we see an oscillation in P_0, noted above. New vortices must appear (not being discussed here) with a period something like this oscillation. Thus, for estimation purposes we estimate a pressure variation with a value peak to peak, see Fig.5, of about 0.05. This would give an RMS pressure normalized by dynamic pressure (which introduces another factor of two) of

$$p_0'/(\tfrac{1}{2}\rho_0 U_0^2) = 0.025\beta\, \mathcal{L}_2^{-1/2}\, 2 = 0.035\beta^2 \tag{25}$$

recalling that our pressure is normalized using βU_0 the span-wise flow speed. The values measured in Refs. [4] and [5] show that P_0 was approximately proportional to U_0^2, as predicted here. The normalized coefficients there ranged from 0.026 to 0.059 in typical circumstance. Obviously the theory fits these experiments quite well. It is difficult to determine the value of β, the span-wise flow intensity, from this portion of the experiment without further treatment of the additional vortices in the problem (a quasi-vortex street).

Our sound measurements in Refs. [1], [4] and [5] were of cross correlations between p_0 the surface, near field, hydrodynamic pressure and p the radiated sound pressure. Consider our large-scale 40 x 80 - Foot Wind Tunnel experiments, see Refs. [4] and [5]. In Fig.6 we show one measured cross correlation. The random fluctuation underlying the correlation peaks is due to the high levels of extraneous noise within the wind tunnel. That background could be removed by taking considerably longer time records during the correlation process. With the funds available we were satisfied with the results shown. The thickness of the flap producing the correlation shown in Fig 6 is approximately 3.2 centimeters. The free stream speed was U_0 = 39.5m/sec. The surface sensor was placed at mid-chord on the first, upstream flap. The far-field microphone for the measurement was located approximately perpendicular to the lower flap surface, in our notation $\theta \simeq 90^0$. The Fig. 6 shows that the normalized cross correlation coefficient is quite small, because of the large background noise levels. There is qualitative resemblance between this cross correlation and the predicted double peak radiated sound, the negative of the R_0 = 2 curve shown in Fig.5. The duration time for the double peak affect is longer, by a factor of five or more, than that measured. To introduce other parameters in the model flow (e.g., shaping the underlying potential flow in the transformed plane) would require other velocity or length scales in the physical flow problem, and at first it seems that none are available. But recalling for example flow around a cylinder we know that behind the object, for Re < 60, there is a pair of vortices bound to the vicinity of the surface--a recirculation. For higher Re (Reynolds number) the vortices are shed and a street is formed. One way of looking at this is the following: Only a weaker vortex can escape the surface and be shed into the street. Thus in modeling the flow, using an inviscid fluid model, we see that the Reynolds' number influences the qualitative characteristics, namely as Re increases the effective vortex strength decreases. It is granted that our Reynolds numbers are considerably larger than those for these flow regimes. Nevertheless, a way out of the paradox above is to adopt the view that even at higher Re there is a weakening of the vortex strength relative to the flow.

It is not difficult to see from Eq.(8) that such a weakening reduces the image-binding effect on the vortex and speeds up the passage time about the corner.

The intensity of the radiated sound was determined in Ref. [4] using three different theoretical methods, which agreed fairly well with one another. We shall use here for reference one of these methods, based upon the surface pressure fluctation p_0. The results for the particular flap being discussed here are shown in Table 1, refer to Eq.(23). We have $\Phi = 0$, $\theta \simeq 90^0$; from the experiment $x_3 = 4m$, $a_0 = 340m/sec$, $c = 0.18m$ and $\rho = 1$ kg/m3. The value of G_H, the negative of the plot Fig. 5 for the curve $R_0 = 2$, is hard to determine without adding further vortices. We take as a nominal figure the peak value of about 0.003. Using the values cited, for the three flow speeds shown in Table 1 we obtain the values of $\beta^3 G_H$ shown in the last column. Evidently the values are slightly high. There are some modifications of the methods used to determine the radiated sound field in Ref. 5, which improve the comparison.

We may sum up as follows: the computations are not extensive for the simple vortex model proposed here. We use but one truly free parameter. The theory predicts surface pressure fluctations well.

The predicted intensity, of the radiated sound field, agrees fairly well with the experiments though it is a little low. Time characteristics of the radiated field match within an order of magnitude but show somewhat slower variation for the theory than is seen experimentally. It is believed that this can be improved by Re effects on vortex strength. It was noted in the treatment that Strouhal numbers less than 1 should be expected in general for flow phenomena of the general class considered here because of the retarding effect of vortex images upon vortex motion. The double peaks appearing in the local and radiated pressure for orbit (b) (in Fig.5) appear to come from the presence of vortex images when the vortex lies near either one of the faces making up the corner. The lack of such well defined images, as the vortex moves past the bisector of the corner increases the surface pressure.

ORIGINAL PAGE IS
OF POOR QUALITY

To compare properly with the sound angular directivity observed in experiments it would be necessary to introduce diffraction effects The presence of the wing can be expected to enhence the normal dipole sound radiated in the up stream direction. This was observed in our experiments, see Ref.[5] and was earlier predicted see Refs. [16]and [17]. The diffraction effect has been recently confirmed in laboratory experiments, see Ref.[18].

The author is indebted to N.M. Nguyen - Vo for the computations presented here.

Appendix A: Sound Calculations and Imcompressible Flow

Lighthill [12] after some manipulation with the exact equations of fluid motion, produces the basic wave equation with source given here in Eq.(1).

In the process of derivation, Lighthill subtracted the quantity $a_0^2 \nabla^2 \rho$ from both sides of the equation. Here a_0, with dimensions of speed, is an arbitrary parameter in the development. No matter what speed is used, the correct result must be obtained when the fluid is compressible. In the usual problem one of course chooses a_0 to be the ambient speed of sound. We make use of the arbitrariness of a_0 in the discussion below.

Curle [13] using the known solution for the wave equation with source, after some manipulation produces the exact result in dimensional form

$$\rho - \rho_0 = (4\pi a_0^2)^{-1} \left\{ \frac{\partial^2}{\partial x_i \partial x_j} \int_v T_{ij} \left(\underline{y}, t - \frac{r}{a_0}\right) \frac{d\underline{y}}{r} \right. \tag{A1}$$

$$\left. - \frac{\partial}{\partial x_i} \int_s p_i \left(\underline{y}, t - \frac{r}{a_0}\right) \frac{dS(\underline{y})}{r} \right\}$$

The first term is the usual volume sound, the second, the surface sound, and

$$P_i = - \ell_j \; P_{ij} \tag{A2}$$

ORIGINAL PAGE IS
OF POOR QUALITY

with ℓ_i the direction cosines of the outward normal, from the fluid. For our discussion it is supposed now that we hava a flow of a slightly compressible fluid, permit the true speed of sound for that fluid to increase without limit, thus approaching an incompressible flow; but suppose that for the calculation of Eq.(A1), the parameter a_0 remains fixed at some finite, ficticious value. The result will be that the left hand side, the density change of Eq.(1), approaches zero. We use the incompressible flow quantities to calculate T_{ij} and P_i. The result is evidently that the two integrals in Eq.(A1) are equal and opposite. The two types of aerosound just cancel one another,

To reemphasize, we expect (using incompressible flow quantities in an aerosound calculation with a ficticious, finite speed of sound) that the surface and volume sound contributions just cancel one another. This result has been checked in at least one situation and found to hold, see Lauvstad and Meecham [15]. In that work a cylinder oscillating (rotating) about its axis and imbedded in an incompressible, viscous fluid produces the expected cancellation.

Appendix B: Relation Between Correlation Width and Spectrum Maximum

Consider a model, broad-band energy spectrum given by

$$E(\omega) = e^{-(\omega - \omega_m)^2/\omega_m^2} + e^{-(\omega + \omega_m)^2/\omega_m^2} \tag{B1}$$

where ω_m is of order the angular frequency of the spectrum maximum. The correlation function is found by taking the Fourier transform,

$$R(t) = \int e^{i\omega t} \; E(\omega) d\omega \tag{B2}$$

The normalized auto correlation is thus

$$[R(t)/R(0)] = \cos(\omega_m t) \exp\left[-t^2 \omega_m/4\right] \tag{B3}$$

We note that even though a Gaussian spectrum centered at the origin has a monotonic correlation function, such a spectrum displaced from the origin has an oscillating correlation function. This is generally true; a spectrum with a maximum displaced from $\omega = 0$ (the typical result in experiments of our kind) will have an oscillating correlation function. No physical model is necessary to explain the observed correlation oscillations.

References

1. Ahtye, W.F., Miller. W.R. and Meecham, W.C., "Wing and Flap Noise Measured By Near-and Far-Field Cross-Correlation Techniques", AIAA Paper 79-0667, Seattle, 1979
2. Fink, M.R. and Schlinker, R.H., "Airframe Noise Component Interaction Studies", NASA, CR-3110, March 1979
3. Kendall, J.M. and Ahtye, W.F., "Noise Generation by a Lifting Wing/Flap Combination at Reynolds Numbers to 2.8 x 10^6. AIAA Paper 80-0035, Pasadena, California, January 1980.
4. Miller, W.R., Meecham, W.C. and Ahtye, W.F., "Large Scale Model Measurements of Airframe Noise Using Cross-Correlation Techniques". UCLA Rept, February 1981; Journal of the Acoustical Society of America, Vol. 71, Pt. 3, 1982. pp. 591-599.
5. Miller, W.R., "Flap Noise Characteristics Measured By Pressure Cross-Correlation Techniques", Ph.D. Thesis, University of California at Los Angeles, 1980.
6. Hayden, R.E., "Noise From Interaction of Flow With Rigid Surfaces; A Review of Current Status of Prediction Techniques", NASA 1-9559-14, January 1972.
7. Yu, J.C. and Tam, C.K.W., "An Experimental Investigation of The Trailing Edge Noise Mechanism", AIAA Paper 77-1291, Atlanta, 1977.
8. Clements, R.R., "An Inviscid Model of two Dimensional Vortex Shedding", Journal of Fluid Mechanics, Vol. 57, Pt. 2, 1973, pp. 321-336
9. Howe, M.S., "Contributions To The Theory of Aerodynamic Sound, with Application to Excess Jet Noise and The Theory of the Flute", Journal of Fluid Mechanics Vol. 71, Pt. 4, 1975, pp. 625-673.
10. Howe, M.S., "The Influence of Vortex Shedding on the Generation of Sound By Convected Turbulence", Journal of Fluid Mechanics, Vol. 76. Pt. 4, 1976, pp. 711-740
11. Hardin, J.C., "Noise Radiation From the Side Edges of Flaps", AIAA Journal Vol. 18, No. 5, May 1980, pp. 549-552
12. Lighthill, M.J., "The Bakerian Lecture, 1961: Sound Generated Aerodynamically", Proceedings of the Royal Society A, Vol. 216. 8 May 1962, pp. 147-182

13. Curle, N., "The Influence of Solid Boundaries Upon Aerodynamic Sound", Proceedings of the Royal Society A, Vol. 231, 8 July, 1955, pp. 505-514

14. Francis, M.S. and Kennedy, D.A., "Formation of a Trailing Vortex", Journal of Aircraft, Vol. 16, March 1969, pp. 148-154

15. Lauvstad, V.R. and Meecham, W.C., "Acoustic Radiation From a Sinusoidally Rotating Circular Cylinder", Journal of Sound and Vibration, Vol. 10, No. 3 1969, pp. 455-463

16. Yildiz, M. and Mawardi, O.K., "On The Diffraction of Multipole Fields by A Semi-Infinite, Rigid Wedge," Journal of The Acoustical Society of Americal Vol. 37 No. 19 1960, pp. 1685-1691

17. Ffowcs-Williams, J.G. and Hall, L.H., "Aerodynamic Sound Generated By Turbulent Flow in the Vicinity of a Scattering Half Plane", Journal of Fluid Mechanics, Vol. 90 Pt. 7 1970, pp. 657-670

18. Meecham, W.C., Bui, T.D., and Miller, W.R. "The Diffraction of Dipole Sound by the Edge of a Rigid Baffle". Journal of the Acoustical Society of America, Vol. 70 No. 5 1981, pp. 1531-1533.

Table 1 radiated sound as measured in the experiment of Refs [4] and [5] from an outboard flap edge, for the upstream, deployed flap.

U_0 (m/s)	SPL at Surface	$\sqrt{p'}$ RMS Value Of p from Ref. [4]	$\beta^3 G_H$ from experiment
39.5	120dB	63dB	0.003
55.8	128	77	0.006
79.0	130	85	0.005

Fig 1. The sketch shows a deployed flap, from the underside of the wing. Two average stream lines are indicated.

Fig. 2. The sketch shows an enlarged view of the deployed flap, with coordinate system indicated. The dashed line shows the projection of $\underline{x}$ in the $x_1 - x_2$ plane.

Fig. 3. (a) A sketch of potential flow about a corner. The dashed line shows the nominal upper surface of the flap. A vortex is shown circulating with the potential flow. (b) Uniform flow in the transformed plane.

Fig. 4. Various orbits for a vortex, imbedded in potential flow about a corner: (a) a vortex passing with $R_0 = 4$ at $t = 0$ ($\theta_0 = -45^0$), (b) a vortex passing with $R_0 = 2$ at $t = 0$, (c) vortex turned back upstream by its image, (d) a vortex counter-circulating under the influence of its image. The divisions between the three flow regimes lie between (b) and (c) and between (c) and (d) respectively.

Fig. 5. Pressure calculations for the two orbits with $R_0 = 2$ and $R_0 = 4$ initially [orbits (b) and (a) of Fig. 4]. The surface pressures, p_0, are plotted using the scale on the right side of the vertical axis and are measured at $y_1 = -0.5$ and $y_2 = 0$, on the flap surface; the pressure when the vortex is distant is used as reference. The quantity $F_{1H} + F_{2H}$, proportional to the radiated sound pressure, see Eq.(16), is plotted using the vertical scale to the left; ——— – ——— gives p_0 for the orbit (a); ——— – - — gives p_0 for the orbit (b); – – – – – – – is proportional to p for the orbit (a) and ——————— is proportional to p for the orbit (b).

Fig. 6. Shows the measured, normalized correlation between a surface sensor placed on the outboard edge of the first flap, in a triple-flap experiment described in Refs. [4] and [5], correlated with a far field mic, located approximately normally to the lower flap surface.

ORIGINAL PAGE IS
OF POOR QUALITY

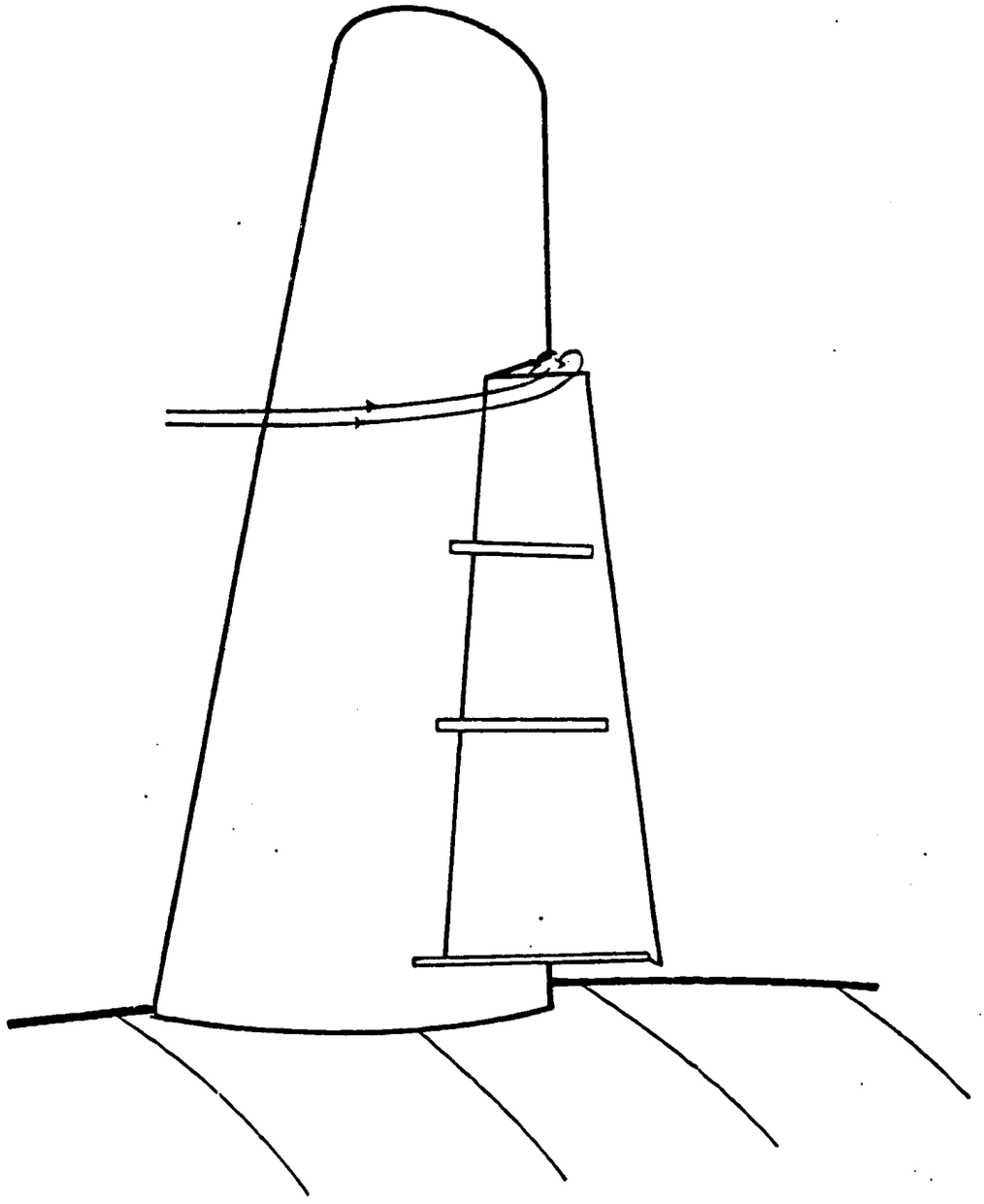

Fig 1

ORIGINAL PAGE IS
OF POOR QUALITY

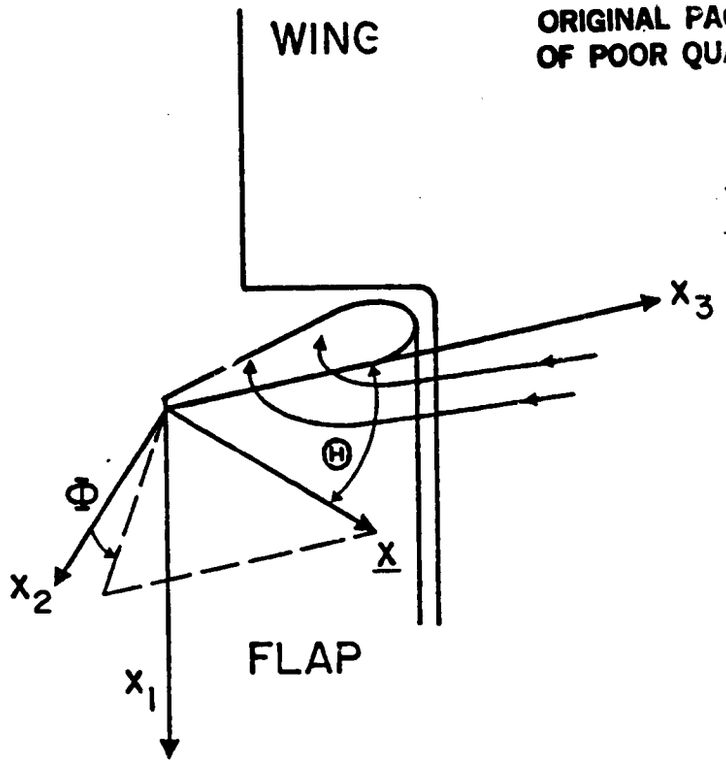

Fig 2

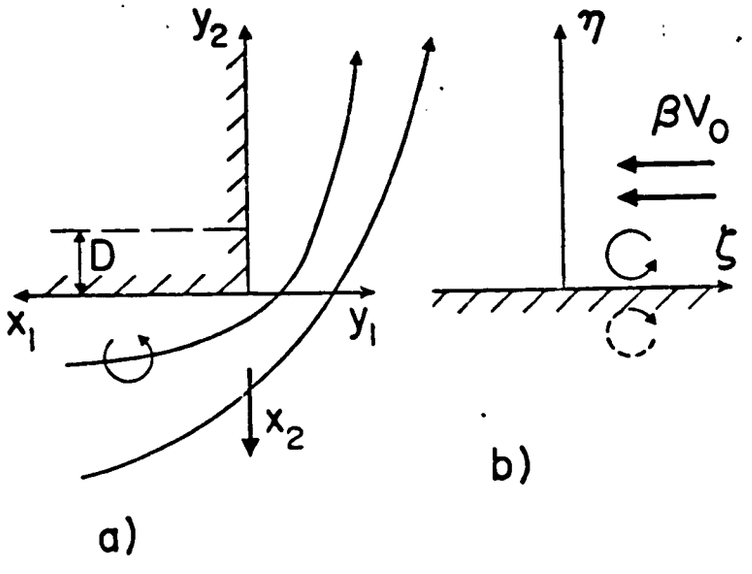

Fig 3

ORIGINAL PAGE IS
OF POOR QUALITY

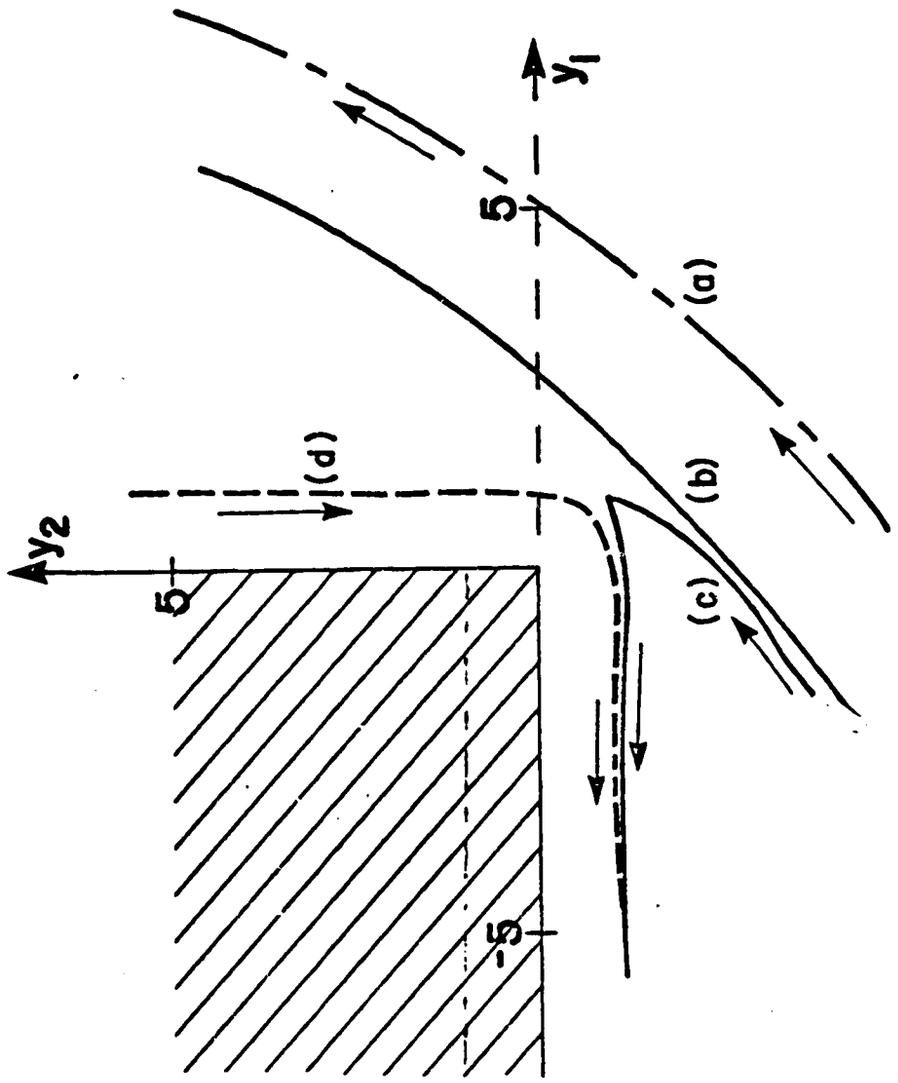

Fig. 4

ORIGINAL PAGE IS
OF POOR QUALITY

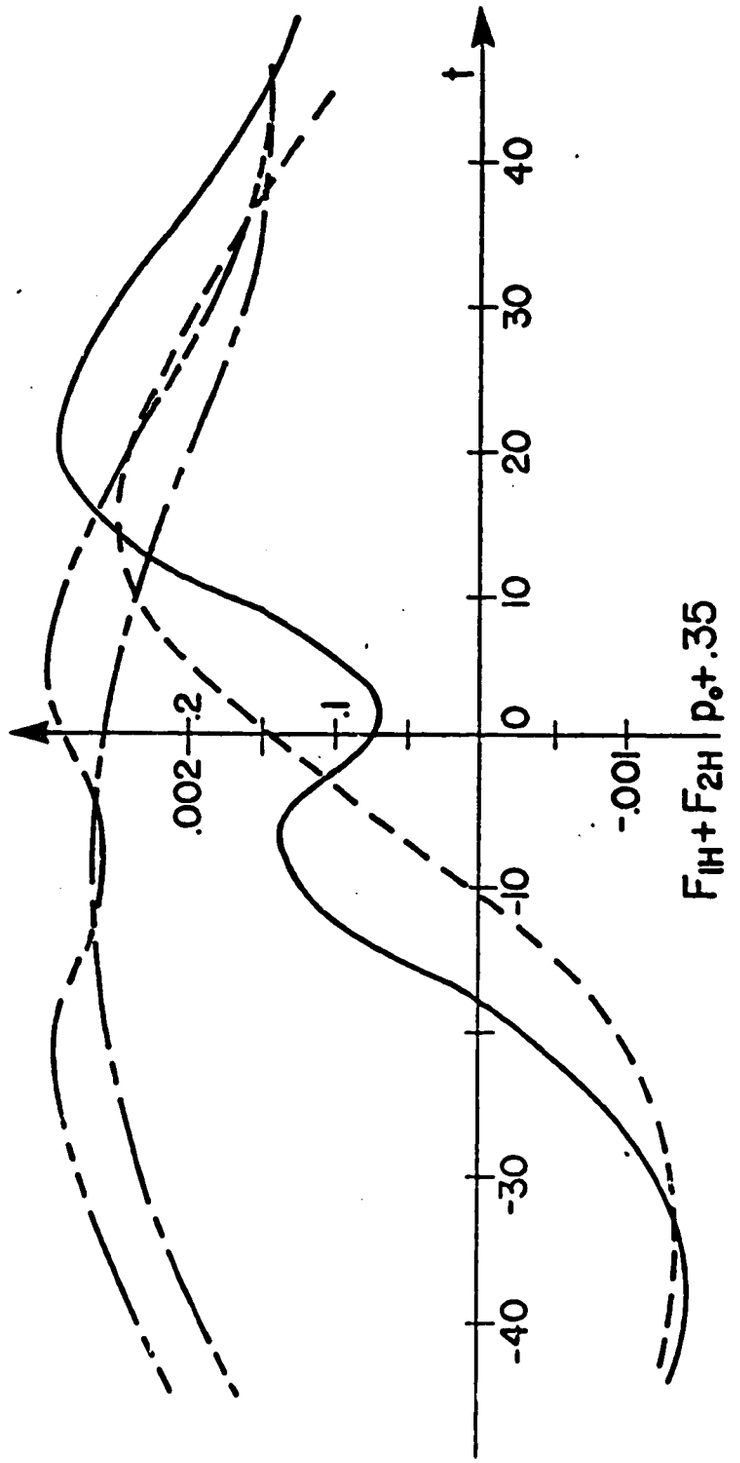

Fig 5

ORIGINAL PAGE IS
OF POOR QUALITY

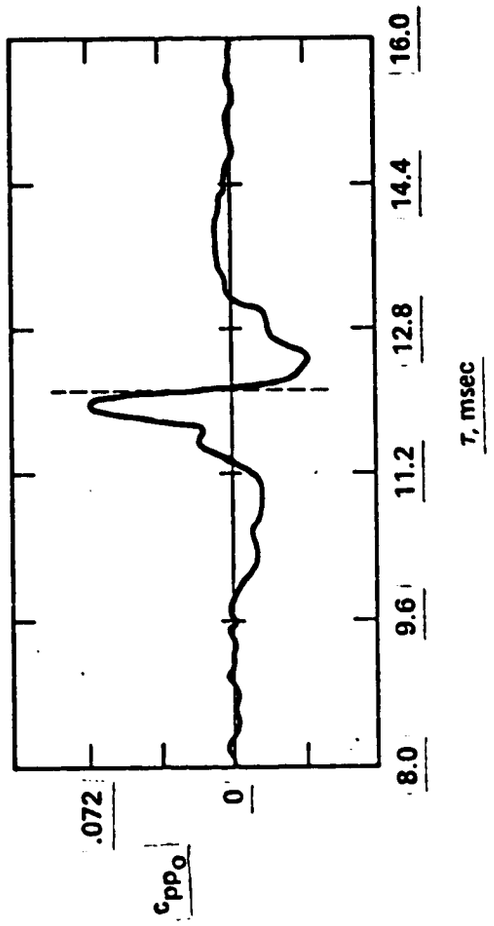

Fig 6

PART II: FINAL REPORT

AEROSOUND FROM CORNER FLOW AND FLAP FLOW, INCLUDING THE EFFECTS OF MULTIPLE VORTICES AND DIFFRACTION

ABSTRACT

Previous work has dealt with surface pressures and radiated sound pressure generated by one vortex moving in potential flow about a corner. We here discuss a model using those results and including the effects of a series of vortices moving in the same idealized potential flow. The procedure essentially supposes that the vortices are statistically independent of one another so that we can add their intensities. We do not include the interaction of pairs of vortices here, supposing that the individual vortices move as they did in the previous report. We take the frequency of appearance of the vortices as determined from measurements. We also add here the diffraction effects ca ed by the presence of the wing near the dipole sound radiators, located on flap surfaces.

Introduction

In Part I a model of the complicated span-wise flap flow around outboard flap edges is proposed. It consists essentially of a potential flow around a corner with a vortex imbedded in that flow. The vortex, of course, generates a quasi-image vortex within the corner surface, which acts to retard the motion of the physical vortex. This moving vortex with its attendant image then produces a time varying pressure variation on the surface of the model of the flap. The result, according to Curle's theory[13] (References are in Part I) is that a dipole source is set up on the horizontal, and another on the vertical, side of the corner. If we suppose that we take our measurements mainly from the underside of the flap, then in principle the dipole set up on the vertical surface has little effect (since we lie approximately in the null plane of such a dipole when directly underneath). Using the time varying pressure it is possible to calculate the radiated sound. There is some difficulty because we use an incompressible flow model for the process. That question is discussed at some length in Part I.

The calculated values for p_o and p, local and radiated pressures, are shown in Fig. 5, Part I, for two different vortex orbits. The preferred vortex orbit, the closer one passing the corner, is the one on which we concentrate here. It is designated orbit (b) in Fig. 4, Part I.

In the work here we have but one parameter β, which can be varied. It is the nominal ratio of the spanwise average flow velocity to the free stream. We also must be given the peak frequency of the local sound pressure variation. That frequency appears in our model as the frequency of repetition of successive vortices. It is hoped that this one parameter and one measurement will be sufficient to describe the sound radiating characteristics of the flap surface. Of course we might obtain the frequency of the local pressure field using a Strouhal number estimate. Here we prefer, however, to use the frequency as taken from measurements which we have available; see Refs. 1 and 4.

I. Surface Pressures

We suppose in this report that we deal with a sequence of eddies passing around the corner, in the potential flow, represented in our model by simple line vortices. We further assume that the individual eddies, circumnavigating the corner, are statistically independent of one another. Then to find the pressure variance for the series of eddies we simply add the variances for each individual eddy at any given time. We also assume that the motion of each eddy is not affected by its neighbors.

There is experimental support for the assumption that the train of vortices (eddies) are statistically independent of one another: The auto-correlation function shows but a single peak [4]. In Fig. 6 (the first six figures are in Part I), we show a typical cross-correlation with demonstrates the essential character of the flow process and suggests that we do not have a coherent train of vortices.

All of the work in Part I was put in dimensionless form using as dimensions βU_o, D and ρ_o; respectively, the span-wise flow (with U_o the free stream), the width of the flap and the ambient density. The resulting pressure in dimensionless form, as measured a distance of 0.5D from the corner on the lower, horizontal surface is plotted in Fig. 5. As said the orbit (b) is preferred. It comes to within 2D of the surface, and is the closest approach which is possible without producing a reverse flow for the vortex. (see Fig. 4). The surface pressure p_o for this orbit is given in Fig. 5 and is specifically the curve for the orbit (b). The radiated sound field pressure is the solid curve for this orbit.

We shall fit these curves using weighted Hermite polynomials. It is seen in Fig. 5 that p_o, the near-field pressure, is approximately symmetrical about a line at time approximately -8 (in dimensional form, $-8D/\beta U_o$). We fit the function p_o using a constant plus even-ordered, weighted Hermite polynomials, all in dimensionless form.

$$10\, p_o = \bar{p}_o + p_2 e^{-\frac{1}{4}\left(\frac{t}{10}\right)^2} He_2\left(\frac{t}{10}\right) + p_4 e^{-\frac{1}{4}\left(\frac{t}{10}\right)^2} He_4\left(\frac{t}{10}\right) \qquad (1)$$

The constants $\bar{p}_o$, p_2 and p_4 are to be determined by fitting the appropriate curve in Fig. 5. To determine these constants we use the values of p_o at the

minimum, at the maximum on the right side and at a distant point (t = 36.3). Furthermore, we can use pressure measurements to obtain the presumed value of β, the spanwise flow speed intensity. We shall distinguish, as discussed below, between the value of β obtained from p_o, call it β_{p_o}, and β_p, that found from the radiated sound field pressure. We refer to Ref. 5 to see the actual measured values of this local pressure field. The results which were presented in Fig. 5.3 of that reference are reproduced here as Fig. 7 (Figs. 7 and 8 are at the end of this Part). One can see the dependence of pressure levels upon the flow speed, and upon position on the flap surfaces. The positions of the measuring points in the flap system, near outer edges, are shown in Fig. 8.

The positions P2, P3 and P4 are essentially equivalent. They lie on the first and second flap. Other positions show lower pressure levels. The dependence of these levels upon the flow velocity is nearly but not exactly quadratic. There is a slight change in the spanwise flow intensity with Mach number (or, alternatively, an increase in turbulence intensity level with Mach number). We find actual power laws for the velocity dependence. Write (primes denote RMS values).

$$p_o' = KU_o^{\gamma}$$

Then using the results in Fig. 7 we find the results shown in Table I

Table I

Dependence of p_o' or U_o

Measurement Position	γ
P5	2.0
P6	2.3
P1	2.5
P2,3,4	2.6

For Eq. (1) we have adjusted the scales in order to have quantities of order unity. Results must be readjusted after the calculation, of course. To find the mean square of the pressure change, due to a large number of statistically independent eddies, we add up the squared pressure changes due to those individual eddies, which occur successively after one another with a period,

T_o. Then the resulting pressure, which is statistically stationary in time, is time averaged and we have the relationship

$$p_o'^2 = (2T)^{-1} \sum_n \int_{-T}^{T} \left[p_o(t-nT_o) - 0.1\, \bar{p}_o \right]^2 dt \tag{2}$$

neglecting end effects (where $|t| \simeq T$) which will be possible if T is large enough, this becomes approximately

$$p_o'^2 = \frac{1}{2T} \frac{2T}{T_o} \int_{-\infty}^{\infty} \left[p_o(t) - 0.1\, \bar{p}_o \right]^2 dt, \tag{3}$$

since all integrals are equal to one another and there are $2\ T/T_o$ of them. Taking the scaling into account and using the properties of the Hermite polynomials in order to calculate the integrals and finally putting results into dimensional form we have the following for the standard deviation (the RMS value) of the near field pressure.

$$p_o' = \rho_o(\beta U_o)^2 \left\{ \left(2!p_2^2 + 4!p_4^2 \right) \frac{\sqrt{2\pi}}{10} \frac{f_o D}{\beta U_o} \right\}^{\frac{1}{2}} \tag{4}$$

where f_o is peak frequency of the flow process (in our model the frequency of repetition of the succeeding eddies). By the described process of curve fitting we find

$$2p_2^2 + 24\ p_4^2 = 0.047 \tag{5}$$

Evidentally, if the Strouhal number, $St = f_o D/U_o$, is approximately constant or but weakly dependent on the flow speed as is to be expected for such flows, the pressure should be proportional to the square of the free stream velocity.

Turn now to the determination of the spanwise flow intensity as obtained from the local pressure fluctuation levels. We shall use the data presented in Fig. 7. The dependence of the levels on flow speed has just been discussed, thus we use the measurements at $U_o = 55.8$ m/s roughly the center of the flow speed range. Referring to Eq. (4) we see that all

quantities are known except a β and T_o. To determine this period we use the cross correlation function reported in Refs. 4 and 5. The general nature of the cross correlation may be seen in Fig. 6. We use the time span between the two negative peaks as a measure of T_o. Measurements from the cross-correlations involved here for the different positions on the flap structure yield values shown in Table II, and using those values and Eq. (4) we obtain the values of beta also shown in that table.

Table II.

Determination of spanwise flow from near field pressure measurements, see Fig. 7

Level of p_o at 55.8 m/R	Measure-ment position	T_o, period of vortex repre-tion	β_{p_o}
111dB	P5	0.70×10^{-3} ms	0.063
123	P6	0.70	0.16
128	P1	0.61	0.22
136	P2,P3,P4	0.80	0.45

The values of the spanwise flow intensity depend on the particular positions on the flaps. The strongest such flows are associated with positions on the first and second of the set.

II. Prediction of Aerosound from Flaps Using the Model of Part I

Using the model of Part I, the resulting density change in the acoustic field is given by Eq. (24) of that Part. The right hand side is plotted in Fig. 5 for two possible orbits. The one farther away from the corner, as shown by the simple dash line of that Figure, and a second orbit (b) shown by the solid line. The second orbit is emphasized, for its behavior is closer to that expected physically.

There is a diffraction effect in the geometry of the flap system. The sources are essentially dipole and their radiation is diffracted by the wing. In the upstream direction, crudely speaking, the wing splits the dipole into its two component parts. As a result, on one side of the wing we see roughly a simple source-like behavior. Down stream we look directly at the dipole,

and far downstream we're in the null plane of that dipole. The effect of this was first described in Ref. [16]. The trigonometric function in Eq. (24) is altered. One replaces $\sin\theta$ by $\cos(\theta/2)$.

We represent the function $F_{1H} + F_{2H}$ by weighted Hermite polynomials as before, using the calculated results shown in Fig. 5. The representation for this function is

$$10^3(F_{1H} + F_{2H}) = \bar{p} + e^{-\frac{1}{4}(\frac{t}{10})^2} \sum_{n=1}^{3} p_n He_n \left(\frac{t}{10}\right) \tag{7}$$

again adjusting the scales to conveniently fit the function. The four constants are determined by fitting the function at the three local maxima and minima nearer the origin and at the distant point of $t = -30.2$.

We include the effect of a train of statistically independent eddies as before, substitute for the diffraction effect just discussed, and calculate the average sound field intensity with due regard to the scaling. Furthermore we write the result in dimensional form. We shall be interested here in sound generated by direct fly over, that is, $\Phi = 0$ (see Part I). The result is

$$I = \frac{(\beta U_o)^6 \rho_o C^2}{x^2 a_o^3}\left(\cos^2\frac{\theta}{2}\right)\sqrt{2\pi}\ \frac{D\cdot 10^{-5}}{\beta U_o T_o}\left[p_1^2 + 2!p_2^2 + 3!p_3^2\right] \tag{8}$$

with C the chord of the flap and where we drop the average value of the pressure field, retaining merely the time varying part, i.e., retaining merely the terms in the sum of Eq. (7). Two observations can be made. First, as suggested in Part I, the intensity is proportional to C^2, with C the chord of the flap. This gives a larger than expected intensity, because the sound source is coherent over the entire flap edge. Second, $T_o \sim U_o^{-1}$ typically (as the flow speed increases, the vortex repetition rate increases). Thus the intensity remains proportional to U_o^6 as expected [10].

For the sum of the squares of the coefficients obtained by the curve fitting process described above, we find

$$p_1^2 + 2p_2^2 + 6p_3^2 = 7.57 \qquad (9)$$

In Ref. 4 three different procedures are proposed for calculating the sound radiated from the whole flap edge, using values measured in those experiments. One of the methods seemed not as effective and won't be discussed here. The other two are discussed in Ref. 4 and results are given there in Eqs. (15) and (17). We shall use those results here. The first of the methods is based upon a use of Curle's formulation [10]. His result is cast in a correlation form and results for the radiated sound are estimated from this form. The second method, designated by the end result Eq. (17) of Ref. [4] relies upon the measured semi-normalized correlation between near field and far field pressures. We shall use the average prediction for these two for comparison with our theory. We'll begin by calculating, using Eq. (8), the value of beta determined from this combination of measured correlations (with some theoretical treatment, in order to deduce total sound radiated by the flap edge). The values of T_o are determined as described above by the cross correlations measured and reported in Ref. 5. The chords of the various flaps are also reported in Ref. 5. The procedure is to use the average sound pressure level (SPL) coupled with Eq. (8) substitute all of the appropriate parameters, and determine the value of β_p from the relation. The results of this procedure are given in Table III.

Surface probe	Farfield mic	U_0(m/s)	Av. $dB_{OBs.}$	C(m)	$Cos^2 \frac{\theta}{2}$	β_p	$I_{predicted}$
P1	M1	39.5	73	0.20	0.55	0.86	72dB
P1	M1	55.8	80.5	0.20	0.55	0.85	80
P1	M1	79.0	89.5	0.20	0.55	0.83	89
P1	M6	39.5	81	0.20	0.88	1.16	73
P1	M6	55.8	86	0.20	0.88	0.86	85
P1	M6	68.4	91.5	0.20	0.88	0.90	89
P6	M1	39.5	63.5	0.31	0.55	0.51	73
P6	M6	55.8	71.5	0.31	0.88	1.80	53
P1	M3	39.5	68.5	0.20	0.33	0.76	70
P1	M3	55.8	76.5	0.20	0.33	0.74	77
P3	M4	55.8	81	0.25	0.70	0.81	81
P3	M3	55.8	75.5	0.25	0.33	0.67	80
P4	M6	55.8	82.5	0.25	0.88	0.76	84
P2	M6	39.5	83.	0.20	0.88	1.06	77
P5	M6	55.8	65.5	0.31	0.88	0.32	86
P6	M6	68.4	77	0.31	0.88	0.50	88
P3	M6	68.4	86	0.25	0.88	0.70	89
P6	M4	55.8	72.5	0.31	0.70	0.46	85
P3	M3	55.8	75.5	0.25	0.33	0.67	80
P1	M4	55.8	84.5	0.20	0.70	0.87	83

Table III

Shows: measured sound levels from flaps, chord lengths, angles, deduced β_p and intensities predicted from an average $\beta_p = 0.81$

The values of beta deduced in this way are evidently higher than the more directly measured ones taken from surface pressure determinations. The conclusion is that perhaps we should think of effective beta for the sound radiation and grant that this will be different than the true spanwise flow intensity. It is encouraging to note the values are not extreme. The average value of β_p obtained from this table is 0.81. Evidentally there is some variation in the proposed values of beta depending on particular flap positions. One way to proceed would be to record these variations and use different values of beta in estimating radiated sound from the various flaps. This, for various reasons, seems at this stage to be unnecessarily complicated. We propose using the single average value. In addition it should be noted that the values of beta determined from surface pressure measurement also showed variation with flap position. In both cases the situation is

complicated by the fact that there was no systematic change. The radiation appearing to be more pronounced from the first and second flap.

We are now in a position to predict the intensity of the radiated sound under the various conditions essentially using Eq. (8) with the average value of beta, 0.81. When this is done one obtains the results shown in the last column of Table III. In the main the predicted sound field intensity is within a decible or two for the first two flaps; there are some excursions for the last flap indicating that a different value of β_p is needed there.

III. Discussion and Conclusions

In Part I we considered the flap-flow model consisting of a simple vortex moving in a potential flow, about a corner. The surface pressure was calculated as a function of time as was the far field sound pressure, the latter obtained using Curle's theory for surface sound. In Part II, we apply these results to the case of a triple flap structure which has been measured earlier. Two main modifications are included. It is supposed that a series of vortices, which are statistically independent, pass about the corner and furthermore we include the effects of diffraction on the radiated sound, the diffraction being that of a dipole source near a wing.

It was found from the measurements that the greatest fluctuations in the local pressure field appeared on the first (leading) and second flap; on these the effective spanwise flow speed intensity was about 1/2. The pressure fluctuation and thus the spanwise flow was considerably less on the third flap (downstream).

In earlier work, the total sound radiated from a single flap was estimated based upon the measured cross correlations of the near-far field pressures. Three different methods were used in that earlier work; two of them seemed close to one another and quite satisfactory. Those are used here. The model which we present in Part I predicts the total radiated sound from the flap surface including its edge and contains a parameter β If we use the theory presented here together with the result obtained through the use of the measured cross correlations found in earlier model work in wind tunnel, we can deduce the effective value of beta. If we use that effective value in the theoretical model we can predict the radiated

sound from the various flap surfaces. This was done; for the strongest-radiating flaps, namely the first and second in the upstream direction, typically the predicted result was within two dB of the result obtained from measurement. The predicted sound radiated from the third flap was not so satisfactory, suggesting that a different value of beta would be needed for that flap. In any event the single value predicts the major part of the radiated sound.

ORIGINAL PAGE IS
OF POOR QUALITY

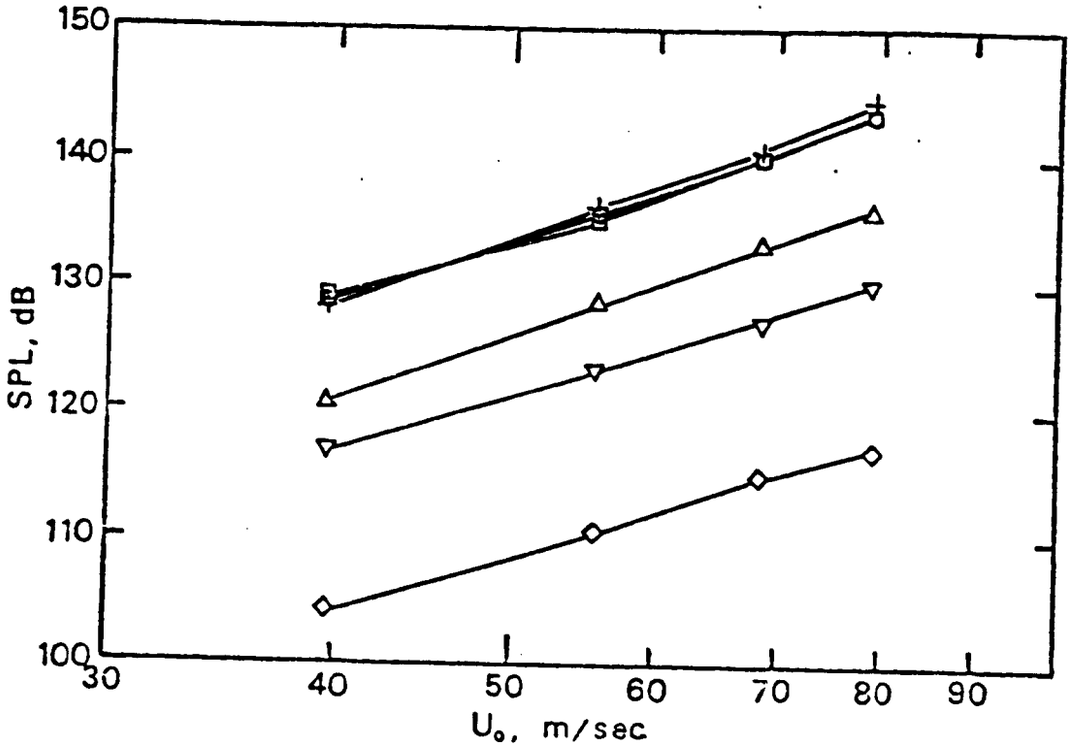

Figure 7. Flap surface pressure levels vs. U_o; levels are referred to 2×10^{-5} Pascals.

ORIGINAL PAGE IS
OF POOR QUALITY

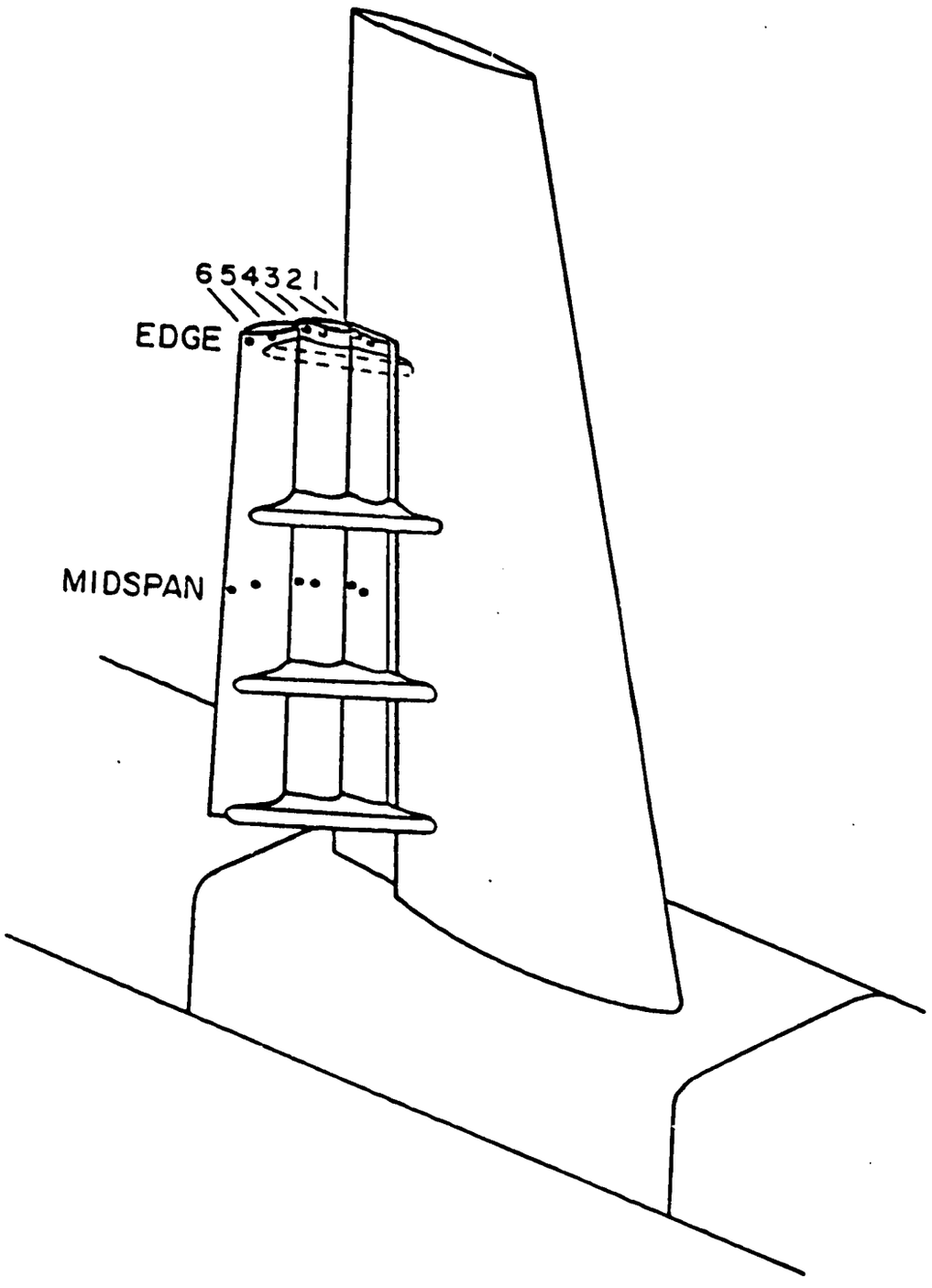

Figure 8. Wing and flap assembly showing local pressure measurement positions.

END

DATE

FILMED

NOV 4 1982